AFRL-AFOSR-VA-TR-2016-0185

Synthetic Aperture Ladar Imaging and Atmospheric Turbulence

Zeb Barber
MONTANA STATE UNIV BOZEMAN

06/09/2016
Final Report

Air Force Research Laboratory
AF Office Of Scientific Research (AFOSR)/ RTB1
Arlington, Virginia 22203
Air Force Materiel Command

REPORT DOCUMENTATION PAGE

Form Approved
OMB No. 0704-0188

1. REPORT DATE *(DD-MM-YYYY)*	2. REPORT TYPE	3. DATES COVERED *(From - To)*
09-06-2016	Final Performance	30 Jul 2012 to 31 May 2016

4. TITLE AND SUBTITLE
Synthetic Aperture Ladar Imaging and Atmospheric Turbulence

5a. CONTRACT NUMBER

5b. GRANT NUMBER
FA9550-12-1-0421

5c. PROGRAM ELEMENT NUMBER
61102F

6. AUTHOR(S)
Zeb Barber

5d. PROJECT NUMBER

5e. TASK NUMBER

5f. WORK UNIT NUMBER

7. PERFORMING ORGANIZATION NAME(S) AND ADDRESS(ES)
MONTANA STATE UNIV BOZEMAN
307 MONTANA HALL
BOZEMAN, MT 59717 US

8. PERFORMING ORGANIZATION REPORT NUMBER

9. SPONSORING/MONITORING AGENCY NAME(S) AND ADDRESS(ES)
AF Office of Scientific Research
875 N. Randolph St. Room 3112
Arlington, VA 22203

10. SPONSOR/MONITOR'S ACRONYM(S)
AFRL/AFOSR RTB1

11. SPONSOR/MONITOR'S REPORT NUMBER(S)
AFRL-AFOSR-VA-TR-2016-0185

12. DISTRIBUTION/AVAILABILITY STATEMENT
A DISTRIBUTION UNLIMITED: PB Public Release

13. SUPPLEMENTARY NOTES

14. ABSTRACT

This is the final technical report for the Air Force Office of Scientific Research Young Investigator Program (YIP) project entitled 'Synthetic Aperture Ladar and Atmospheric Turbulence'. It includes a technical summary of the entire effort and a more detailed description of the final portion of the effort. The overall objectives of the effort were to utilize high resolution FMCW ladar techniques for high resolution synthetic aperture ladar (SAL) imaging as a tool for investigating atmospheric turbulence, and investigating the effect of atmospheric turbulence on coherent ladar and SAL imaging. The main concept for investigating turbulence using the high resolution FMCW ladar was to use range resolved point targets (retroreflectors) as beacons in a two-way ladar measurement system.

15. SUBJECT TERMS
LADAR

16. SECURITY CLASSIFICATION OF:			17. LIMITATION OF ABSTRACT	18. NUMBER OF PAGES	19a. NAME OF RESPONSIBLE PERSON
a. REPORT	b. ABSTRACT	c. THIS PAGE			MOSES, JULIE
Unclassified	Unclassified	Unclassified	UU		19b. TELEPHONE NUMBER *(Include area code)* 703-696-9586

Standard Form 298 (Rev. 8/98)
Prescribed by ANSI Std. Z39.18

Final Technical Report (& final update for August 2015-May 2015)

(YIP) Synthetic Aperture Ladar Imaging and Atmospheric Turbulence FA9550-12-1-0421

Author(s) of Report:
Dr. Zeb Barber, PI Montana State University,
Jason Dahl, Contributor Montana State University

Principle Investigator:
Dr. Zeb Barber
Director MSU-Spectrum Lab
Montana State University
PO Box 173510
Bozeman, MT 59717
barber@spectrum.montana.edu

Contract Representative:
Naomi Stewart
Office of Sponsored Programs
Montana State University
307 Montana Hall
Bozeman, MT 59717
nstewart@montana.edu

Abstract

This is the final technical report for the Air Force Office of Scientific Research Young Investigator Program (YIP) project entitled "Synthetic Aperture Ladar and Atmospheric Turbulence". It includes a technical summary of the entire effort and a more detailed description of the final portion of the effort. The overall objectives of the effort were to utilize high resolution FMCW ladar techniques for high resolution synthetic aperture ladar (SAL) imaging as a tool for investigating atmospheric turbulence, and investigating the effect of atmospheric turbulence on coherent ladar and SAL imaging. The main concept for investigating turbulence using the high resolution FMCW ladar was to use range resolved point targets (retroreflectors) as beacons in a two-way ladar measurement system. The statistics of the phase and amplitude fluctuations of the beacon signals can then be used to measure the strength of the optical turbulence in the path. In addition, to investigating the effects of atmospheric turbulence on SAL imaging through simulation, optical hardware was constructed to implement and investigate the Differential Synthetic Aperture Ladar (DSAL) imaging, which may have advantages over standard SAL imaging in the presence of turbulence near the target. In the period since the last progress report, we have improved the DSAL hardware and performed comparison measurements between more standard SAL imaging and DSAL in the presence of different atmospheric turbulence conditions. Also during this final period we improved upon the measurement setup and data processing methods for the FMCW ladar based atmospheric turbulence measurement tool that allows us to have better confidence in our measurement of atmospheric turbulence.

Table of Contents

Project Outputs this Reporting Period

Student Training

One graduate student in Optics, Chris Ross Blasczyzk, was supported on this project during this reporting period. Ross just completed his first-year in the MSU Master's in Optics and Photonics program and performed work on turbulence characterization supported by the YIP for the fall semester. During the spring semester he was supported by an Air Force Phase II SBIR to further develop the turbulence characterization methods began with the YIP. This summer he will be working on a summer internship with Blackmore Sensors and Analytics, (formerly part of Bridger Photonics, Inc.). His Master's thesis should be completed in the spring semester 2017, with his thesis topic being atmospheric turbulence characterization using coherent ladar.

Presentations

"FMCW Differential Synthetic Aperture Ladar for Turbulence Mitigation," Zeb Barber, Jason Dahl, and Christopher Ross Blaszczyk. 18th Coherent Laser Radar Conference, June 26-30, 2016 Boulder, CO USA (Invited Presentation)

Published Archival Papers

Crouch, S., Kaylor, B. M., Barber, Z. W., and Reibel, R. R. "Three Dimensional Digital Holographic Aperture Synthesis" Optics Express 23, no. 18 (2015): 23811. doi:10.1364/OE.23.023811, Available at https://www.osapublishing.org/abstract.cfm?URI=oe-23-18-23811 (Z.W. Barber's contributions).

Other Synergistic Activities

Dr. Barber was a Co-PI on an Air Force Phase II SBIR with Blackmore Sensors and Analytics (formerly part of Bridger Photonics, Inc.) entitled "Tomographic Coherent Ladar Based Atmospheric Turbulence Profile Characterization System". This SBIR project augmented the YIP effort and involved transferring some of the technology and techniques developed on the YIP effort, including the phase based turbulence measurement methods and processing techniques. The ideas for the SBIR were first explored on the YIP, and if successful it may lead to the delivery of an atmospheric turbulence characterization system designed for coherent ladar, that will help the AFRL coherent ladar groups better characterize their ladar and ladar imaging systems.

A second synergistic activity was that Dr. Barber taught a graduate level course in the "Numerical Wave Optics Simulation" for the Electrical Engineering Department. This course had an enrollment of five students and taught them how to perform numerical Fresnel propagation simulations including simulating propagation through atmospheric turbulence. The course work made extensive use of the MATLAB programming environment with similar functions and programs as developed during this YIP project.

Technical Progress

Background

The objective of this Young Investigator Program project is to study the intersection of synthetic aperture ladar (SAL) and atmospheric turbulence. SAL is a range imaging modality that is the optical equivalent of synthetic aperture radar (SAR), which has been deployed for a number of applications since the 1960's. Investigations into SAL have been sporadic, with some early studies[1] and some more recent studies including most recently a successful demonstration of SAL image formation from a flying platform[2], [3]. One of the main difficulties that have held back SAL is a lack of stable, broadly-tunable laser sources for chirped FMCW ranging. It was through this direction[4] that Dr. Barber and MSU-Spectrum Lab entered the field of high resolution SAL imaging along with our small business partner Bridger Photonics. Since then we demonstrated table-top and longer distance SAL imaging[5]. During the longer distance SAL imaging demonstrations we noticed the significant deleterious effect of turbulence on the SAL imaging, only being able to form images during periods of low turbulence. This then was the motivation of this effort – use the tools we had developed for high resolution SAL imaging to study turbulence and in turn use that new knowledge to improve the performance of high resolution SAL imaging.

Technical Progress by Objective

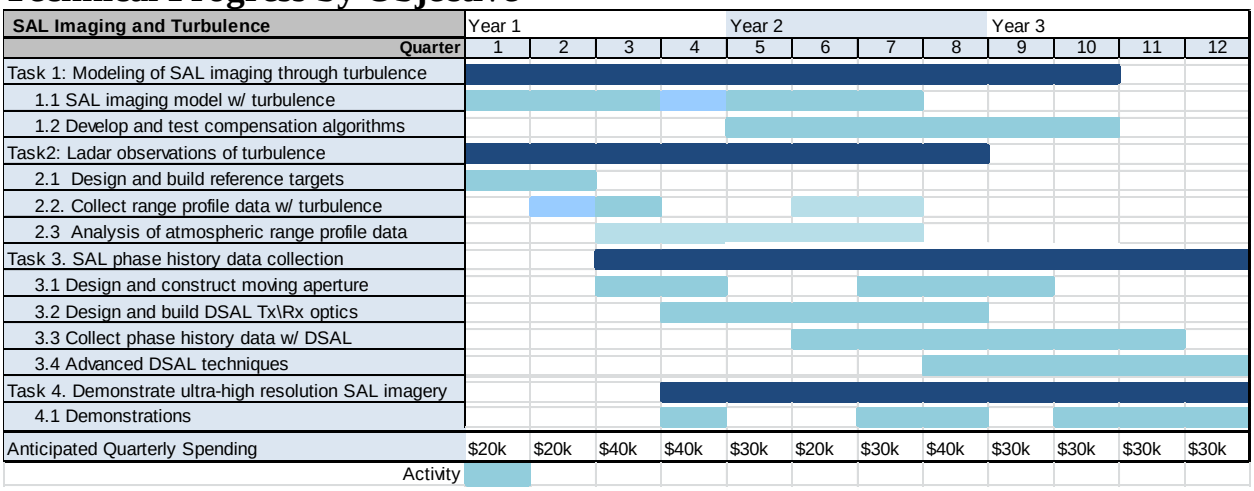

Figure 1 Gantt chart outlining the objectives and tasks as originally planned.

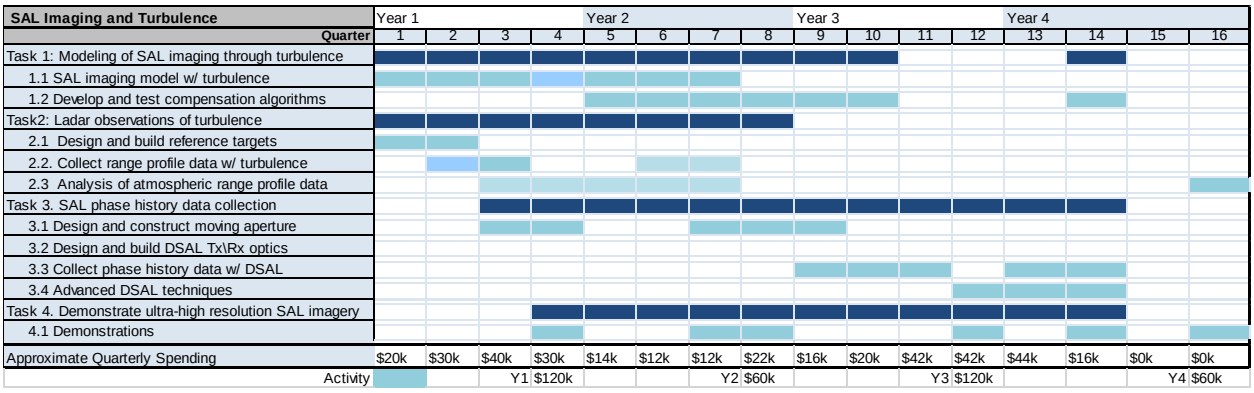

Figure 2 Gantt chart outlining objective, tasks, and spending reflecting actual progress including the No Cost Extension. As can be see the main shortfall that led to the NCE occurred in the 2nd year of the effort. Although the project was extended for 1 year, the funds were expended in 6 months.

Task 1: Modeling of SAL imaging through turbulence

This objective and sub-tasks were completed mainly in the first year; however, the tools developed were used to investigate and analyze the turbulence and DSAL imaging. The main tools and accomplishments under this task include: development of full frequency dependent beam propagation and SAL signal simulation with the inclusion of turbulent phase screens. This model\simulation was used to develop realistic SAL simulations and to investigate the deleterious effects of turbulence. The simulation and model was developed in MATLAB and later revisions of the model made in Years 2 and 3 of the project included GPU implementation of the beam propagation using the parallel processing toolbox in MATLAB. The use of a GPU greatly decreased the run-time of the SAL simulation from several hours to several minutes for relatively large SAL images (300x300). A summary of some of the results are included below.

Task 1.1: SAL imaging model w/turbulence Status

In developing the SAL simulation two different optical beam propagation methods were explored, which were described in a previous report as the Fourier Optics beam propagation (Angular-Spectrum Propagation) and the Fresnel beam propagation (Fresnel Integral Computation) methods. These beam propagation methods serve as a module in the larger SAL simulation program and is shown in Figure 3. The SAL simulation consists of two loops that produce a 2D matrix representing the phase history data for the SAL processing. The two dimensions are the wavelength or frequency of the laser, which corresponds to time for linear frequency chirps, and aperture position. Kolmogorov spectrum turbulent phase screens and modified Hill spectrum phase screens could be used; however, little difference in effect on the phase history data or SAL imaging was discernible.

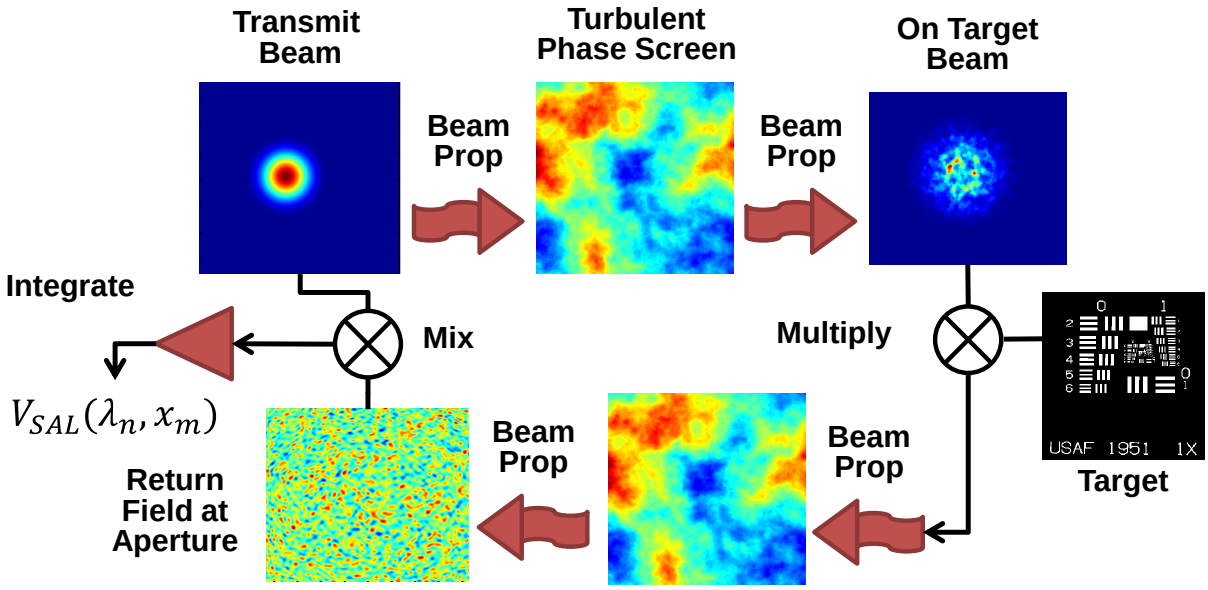

Figure 3 Schematic showing a block diagram for the main sequence block of the SAL simulation. This block was repeated for every transmit beam position (x_m) and frequency step (λ_m) of the optical chirp to capture the complete phase history data.

Task 1.2: Develop and Test Compensation Algorithms

Figure 4 shows an example output of the SAL simulation. This includes a SAL image with a single thin turbulent phase screen with a C_n^2 value of $1x10^{-14}$ placed near the aperture. One can see that the turbulence only has the effect of causing blurring in the cross-range dimension (horizontal in the images). Additionally, one can see that the Phase Gradient Autofocus (PGA) algorithm is quite effective at compensating for the turbulence when the phase screen is near the aperture. If the phase screen (or distributed phase screens) were located further away from the aperture the tilt caused by the turbulence becomes significant and PGA had a more difficult time compensating effects of turbulence. Conclusions reached with these SAL simulations was that the effect of a thin turbulent phase screen was strongest near the aperture and decreasing as it neared the target. However, the Phase Gradient Autofocus (PGA) algorithm, which was first developed for SAR phase compensation, proved most capable of correcting errors due to a turbulent phase screen near the aperture, PGA was less effective the closer the phase screen was to the object.

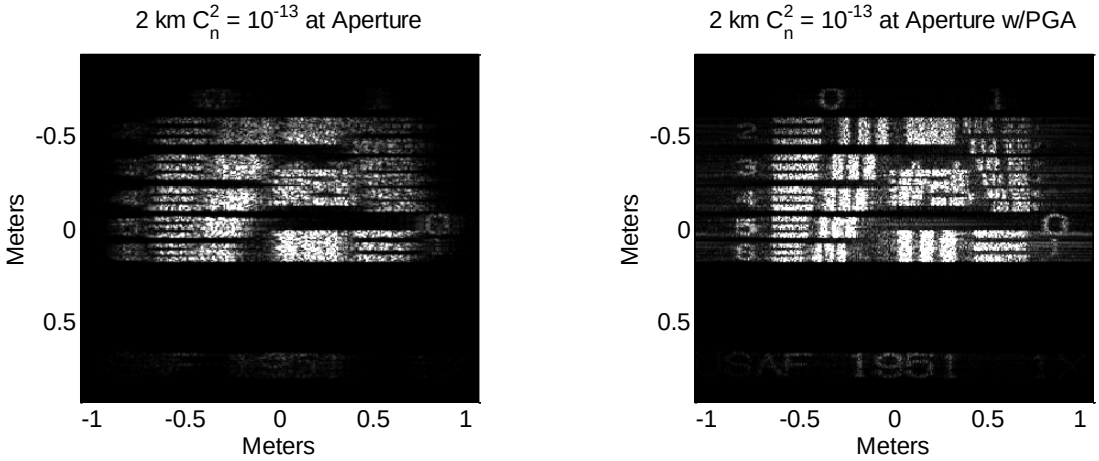

Figure 4 SAL simulation output for placing the turbulent phase screen near the transmit\receive aperture using no autofocus algorithms in the SA processing (left) and using the phase gradient autofocus (PGA) algorithm to help focus the image (right). As one can see the PGA algorithm is capable of compensating for significant turbulence induced defocusing.

Task 2: Ladar observations of turbulence

While this task was basically completed in the first two years of the effort, we revisited this task in late 2015 and early 2016 and have developed some better measurement and processing methods. These methods are being transferred to industrial partner Bridger Photonics and will be developed further during an AF Phase II SBIR to help the AFRL EO Sensors group at WPAFB to characterize the atmosphere during tests of coherent ladar imaging systems. The development of this technique is a main technical outcome of this YIP project. The older work is summarized for completeness and the more recent work is described in further detail below by task.

Packaging of Stabilized Chirped Laser

While not a specific task, two improvements were made to our high resolution ladar source during this project that made it more suitable for the ladar based turbulence characterization measurements and the SAL and DSAL measurements under Objective 3. This stabilized chirped laser system is based on a commercially available tunable DFB (distributed feedback) laser at 1536 nm and the stabilization techniques developed at MSU. The system was made more compact by removing the need for an external timing generator to control the timing of the chirps. The timing generator was replaced by clocking an internal microcontroller to a stable clock and using one of the general input/output pins. This allows the chirp laser system to be completely standalone. The second improvement made to the chirp laser system was to implement a center

frequency lock to a molecular absorption line in Hydrogen Cyanide (HCN). This keeps the absolute center frequency of the chirp from drifting which leads to undesirable phase drifts on the FMCW ladar measurements.

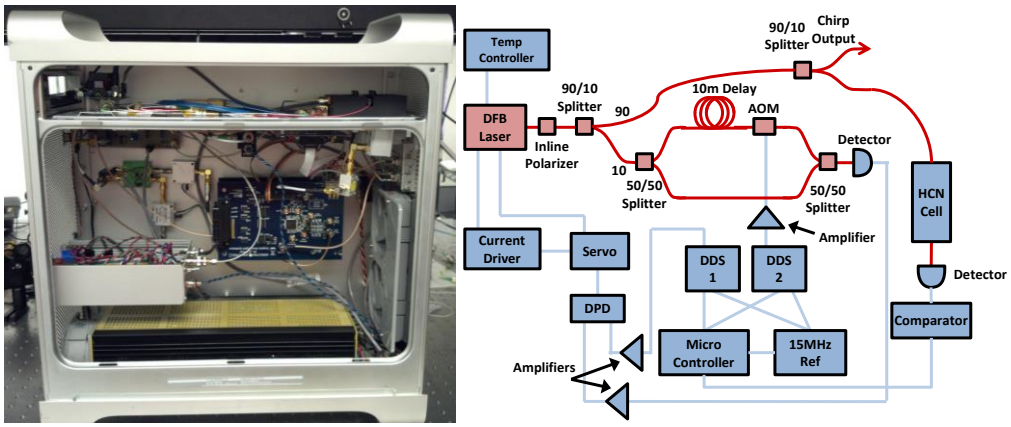

Figure 5 (Left) Packaged stabilized chirped laser system. From left to right: front, back, and inside views. (right) Design of the stabilized chirped laser at 1536 nm. DFB: distributed feedback laser, AOM: acousto-optic modulator, DDS: direct digital synthesizers, DPD: Digital Phase Detectors

Task 2.1: Design and build reference targets

Figure 6 is a picture of the raging/imaging system on a small wheeled optical table which includes the chirp laser, optics and other necessary hardware including a motorized translation stage for synthetic aperture formation. It also included examples of the test targets available for the turbulence and SAL imaging studies.

Figure 6 Portable ranging/imaging system and target system on tripod with gridded ball retro targets and a target pattern constructed of retro-reflecting tape for SAL and DSAL studies.

Task 2.2: Collect range profile w/ turbulence

Y1&2

Using the portable ranging/imaging system shown in Figure 6 we performed data collections of the range profile of the target shown in Figure 7 at different distances 25, 50, and 100 meters over an asphalt parking lot. The data was collected, FFT'd and windowed around the target range, to reduce data storage requirements. Further processing was done in post to fit the target profiles for

the multiple targets to extract the phases and intensities then remove the common mode phase fluctuations. Analysis of the statistics of the target phase and intensity fluctuations was then performed to connect back to C_n^2 values. Unfortunately, comparing this to ground truth was difficult and even measurements at the daily sunrise and sunset and minima seemed inconsistent.

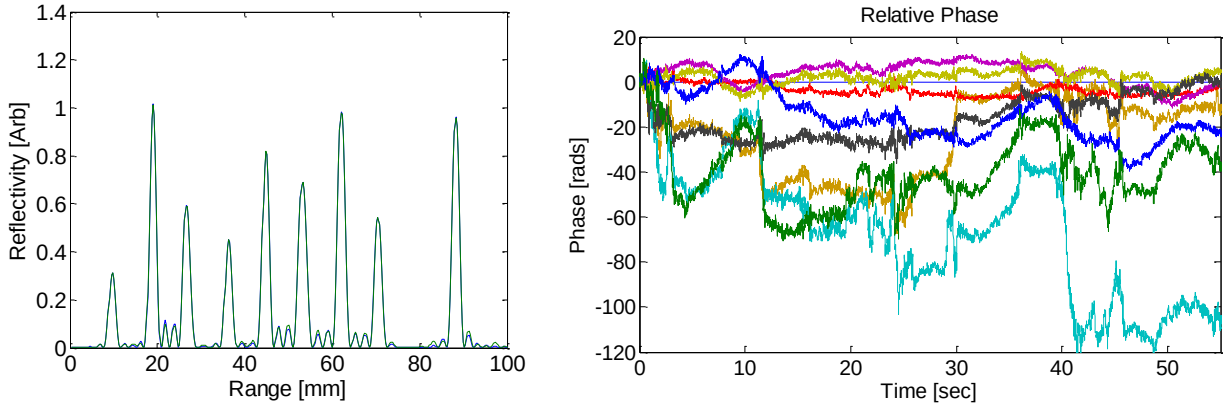

Figure 7. (Left) Range profile of nine cat-eye retro-reflector targets equally spaced in range randomly placed in the transverse directions. The target array was placed 25 meters away on a sunny day over black top to produce strong turbulence. (Right) The relative phase evolution of the individual targets referenced to the target at the farthest range. Using the log variance of the received signal power over the 50 seconds and the simplified expression in [6] gives C_n^2 estimate for this data set of approximately 10^{-12} $m^{-2/3}$.

Sept 2015 – Feb 2016

In the fall of 2015, upon our discovery of the ability to produce real atmospheric turbulence in a controllable manner using a simple space heater, we revisited the use of the high resolution FMCW ladar as a tool for characterizing atmospheric turbulence. The earlier efforts used a target with a relatively few number of retroreflectors and while able to track the phase and amplitude of these targets, the best way to process them to extract turbulence strength values such as r_0 or C_n^2 values was elusive. Calculating values based on (see Figure 7) amplitude scintillation seemed to produce values that were reasonable (near the right order of magnitude), but there was little way to verify that we were getting the right answer and attempts to process the data based on the phase evolution ran into problems with figuring out how to properly deal with things such as phase unwrap errors. In addition, to this we felt that the estimates could be improved by use of more retro-reflectors. For this reason we constructed new targets based on a square grid of retro-reflectors spread out in range space so that each retro is well resolvable (see Figure 8). After constructing the target we hit upon the method to generate realistic turbulence in a laboratory environment with the simple use of an electric space heater. The space heater creates a large temperature gradient which leads to real dynamic atmospheric turbulence. This allowed to test our data processing methods with a controllable source and was crucial to developing the processing method based on structure functions described below.

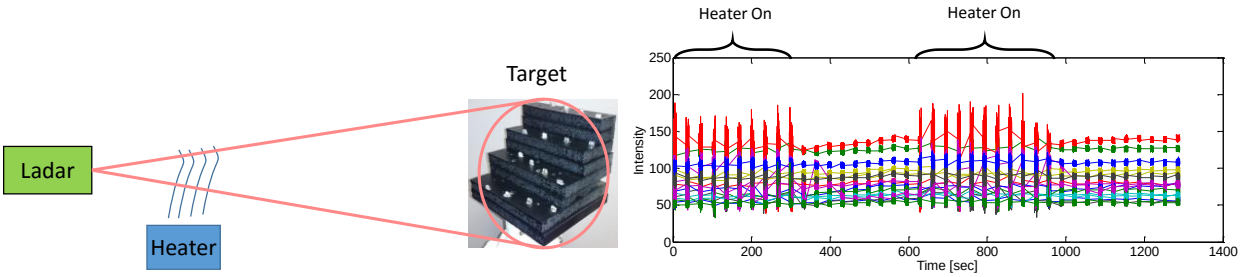

Figure 8 (Left) Simple diagram of turbulence measurement setup. (Right) Peak intensity for each retro-reflector for each FMCW chirp measurement. There are 2000 chirps in each bunch in time and 40 separate iterations were made over about 20 minutes with the heater being on-off-on-off.

In the Kolmogorov regime, the wave structure function for a plane wave propagating through optical turbulence is:

$$D\left(\vec{r},\vec{r'}\right) = \int \left[U(\vec{r}) - U\left(\vec{r'}\right)\right]^2 d\vec{r} = 6.88\left(\frac{r}{r_0}\right)^{5/3}.$$

So the structure function defines the statistical two point differential variance of the optical field as a function of the separation. So if one were able to measure the variance of the optical field as a function of separation one could fit the data to extract a value for r_0 and thus the strength of the turbulence. By comparing the relative evolution of phase and amplitude of the FMCW returns from two retro-reflectors separated by a distance r_{jk} one gets a single estimate of the structure function at that separation. With a target of a 4x4 square array one can generated 16^2 = 256 different estimates of the value of the structure function at different separations ranging from a unit distance to ~5.7 units (the diagonal). These structure function estimates $D\left(r_{jk}\right)$ can then be fit with the form above to provide a better estimate of r_0. One of the issues with calculating the structure function for our setup is that due to unavoidable small range offsets the returns from each retro-reflector have an overall random phase. First attempts to correct for this was to estimate the mean phase difference of each retro-reflector, subtracting this from the overall calculation of the phase variance. Further investigation pointed us to the use of mutual coherence as a better method to estimate the value of the structure function. The mutual coherence of two points $\vec{r},\vec{r'}$ is defined as:

$$\Gamma\left(\vec{r},\vec{r'}\right) = \langle U(\vec{r})U^*(\vec{r'})\rangle = U_0(\vec{r})U_0^*\left(\vec{r'}\right)\langle \exp\psi\left(\vec{r}\right)\exp\psi\left(\vec{r'}\right)\rangle,$$

where U_0 is the field without turbulence and $\psi(\vec{r})$ is the Rytov perturbation due to the turbulence. This mutual coherence function can be normalized to calculate what is known as the modulus of the complex coherence factor

$$\mu\left(\vec{r},\vec{r'}\right) = \frac{\left|\Gamma\left(\vec{r},\vec{r'}\right)\right|}{\left|\Gamma(\vec{r},\vec{r})\Gamma\left(\vec{r'},\vec{r'}\right)\right|^{1/2}}$$

Which is related to the wavestructure function as $\mathrm{D}\left(\vec{r},\vec{r'}\right) = -2\ln\mu\left(\vec{r},\vec{r'}\right)$. What is nice about using the modulus of the complex coherence factor is that it is independent of the overall relative phase and amplitude of the two field points. This can be seen in Figure 9 that shows how the complex coherence factor is a measure of the distance from the origin that results from summing the relative phasors. For perfect coherence the coherence factor has unity modulus. So the data processing procedure proceeded as: 1) Extract the amplitude, a, and phase, ϕ, of the FMCW range return for each retro-reflector and form a time evolving field estimate for the jth reflector-return as: $U_j(t) = a(t)\exp i\phi(t)$. 2) Calculate the complex coherence factor for every retro-pair

combination $\mu_{jk}(r_{jk})$ and the corresponding value of the structure function. 3) Fit these $D(r_{jk})$ points to a 5/3 power law and estimate the resulting r_0. The various stages of this calculation are plotted in Figure 9.

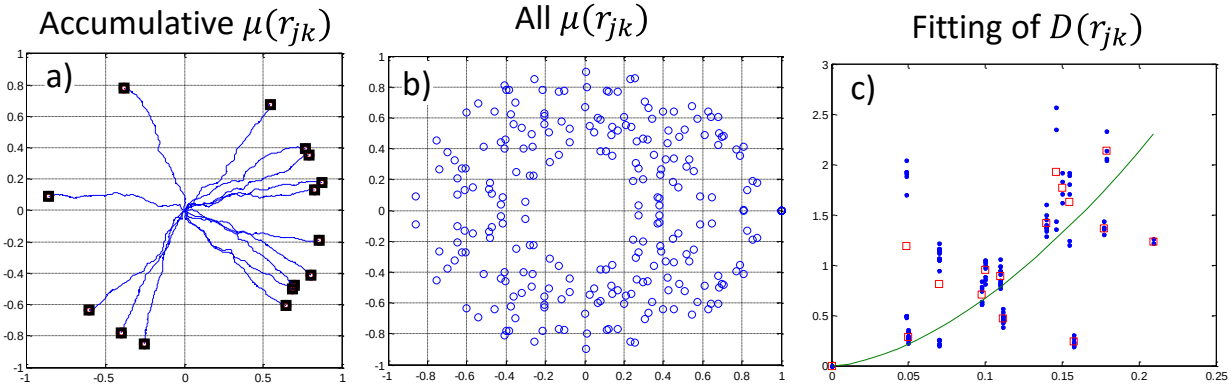

Figure 9 a) This figure shows how the mutual coherence can be thought of as an accumulative phasor sum that evolves further from the origin the more mutually coherent the two points are. Phasor sums shown here are for a few retro-pairs relatively weak turbulence condition. b) This figure shows the measured complex coherence factor values for every retro-pair at the same turbulence condition. As can be seen the largest values of $\mu(r_{jk})$ lie near the unit circle. c) The structure function values calculated from the b) are the blue points. The green line is the power law fit to the points and the red squares is the mean value of the structure function over the different pairs with the same separation. The 5/3 fit seems reasonable.

To test this data processing method we were able to generate consistent C_n^2 values for the tests with the space heater as a source of turbulence. Figure 10shows the measured C_n^2 values for different positions of the space heater. One issue with this estimate is that the approach is based on assuming the phase variance of the double pass propagation is just twice that of single pass propagation, the second issue is that the transverse spacing of the retro targets was ~ 5 cm, which was too large for the strongest turbulence causing a saturation of the measured C_n^2 values. Despite these issues this method seems to be a promising approach to characterize atmospheric turbulence using coherent ladar which will allow it to extend to very large distances.

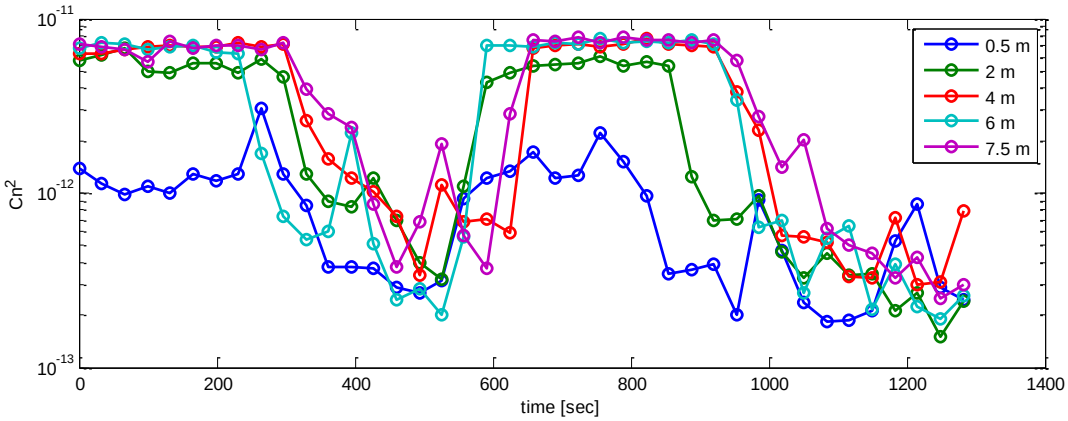

Figure 10 The measured C_n^2 values as a function of time with the on-off-on-off pattern of the space heater for different positions of the space heater as measured from the FMCW ladar Tx/Rx aperature.

Task 3: SAL phase history data collection

This objective was fairly successful with two main accomplishments. 1) We constructed, tested, and experimentally demonstrated a high resolution Differential SAL (DSAL) imaging receiver. 2)

We tested the DSAL imaging receiver in the presence of real optical turbulence and compared its performance to more standard SAL image processing using the PGA algorithm. While the DSAL was first demonstrated in 2014 on the project, we redesigned the DSAL receiver twice to improve the compactness and performance, and completed the comparison of the DSAL and standard SAL processing methods in the Fall of 2015. The results prior to Sept 2015 are summarized below and more detailed work performed in the final reporting period is presented in more detail.

Introduction to DSAL

Synthetic Aperture Ladar (SAL) provides image resolution beyond the standard diffraction limited resolution of the physical optical aperture by utilizing relative aperture\target motion. Two of the key capabilities required for SAL imaging[7] are: 1) a coherent ladar system with large waveform bandwidth to provide range resolution at the desired image resolution; and 2) the ability to correct the inevitable phase errors that arise during the aperture/object motion. The first capability was largely solved from prior efforts through the development of stable and linear frequency modulated continuous wave (FMCW) ladar sources with up to sub-100 micron resolution [4]. The second capability at first appears extremely difficult as naively it means maintaining holographic stability between the measurement system and the object, which can be separated by large distances. Fortunately, we have found that the phase gradient autofocus (PGA) algorithm, an image based correction algorithm, works incredibly well to estimate the shot-to-shot piston phase errors and focus the SAL image. PGA uses the fact that the largest phase errors are due to piston motion (on the axis between the target and the receiver) which is common mode to the entire scene. It then uses bright scatterers of opportunity in the image as phase references to estimate the phase errors and applies the corrections in an iterative fashion.

Differential SAL (DSAL) is an alternative, hardware based technique to compensate pulse-to-pulse phase errors that was proposed and patented in 2005 [4]. To the best of our knowledge, no experimental demonstrations of the DSAL technique have been performed before our own presented here. The idea behind the DSAL technique is to measure the derivative of the range resolved signal phase rather than the absolute optical phase at every aperture position. The phase evolution across the synthetic aperture can then be reconstructed by numerically integrating this derivative. In this respect, it is very similar to the PGA algorithm where one of the steps of the algorithm is to estimate this derivative of the phase. In the original DSAL paper [8], this measurement is performed by physically dividing the real aperture into a left and right half along the direction of motion and detecting the signal using heterodyne detection in each half separately. The differential phase between the two halves of the aperture provides the estimate of this derivative.

DSAL purports to have several benefits including: 1) Inherent insensitivity to line-of-sight motion, greatly reducing the requirements on stable motion. 2) Single pulse measurement of the phase derivative reducing sensitivity to changing phase errors introduced between pulses such as that due to non-static atmospheric turbulence. 3) Phase derivative estimate is made for each range line simultaneously, which means range dependent phase errors are estimated separately unlike with PGA. The tasks below describe the efforts made to implement DSAL experimentally in the lab, compare it with PGA based phase error compensation, and ongoing efforts to take synthetic aperture imaging experiments to longer ranges (>100 m) while maintaining high resolution.

Task 3.1: Design and construct moving aperture.

See Task 3.2

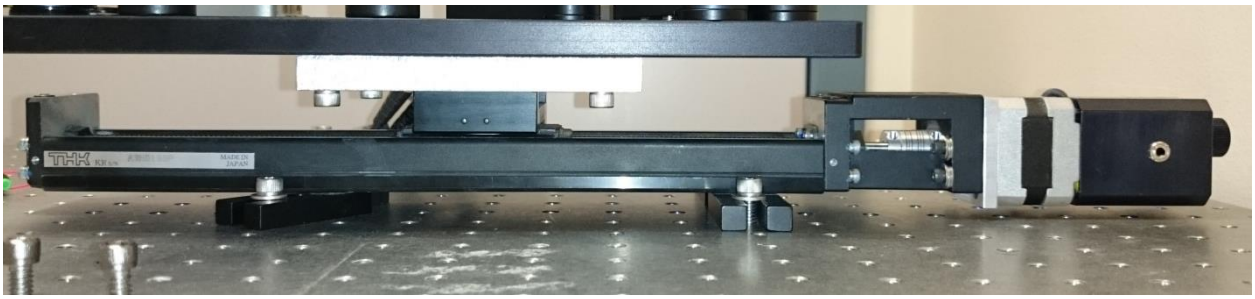

Figure 11 The translation stage and Zaber motor used for the moving aperture.

Task 3.2: Design and build DSAL Transmit\Receive optics.

The design of the Differential SAL (DSAL) Tx\Rx optics has undergone a few revisions in order to make it more compact and stable. The current design utilizes polarization to recombine the LO and receive beam onto two quad cell photodetectors that are wired differentially to provide residual intensity noise suppression. Figure 12 shows a schematic of the optical system. A chirped DFB laser at 1536nm is split in fiber to provide the ability to adjust the relative delay of the LO and signal path. The majority of the laser power is directed to the signal path where it is focused using a 50 mm lens to create a small effective aperture. A small aperture is needed to produce a usable spot size (which limits the image field of view) on the target. The return energy is directed toward the detectors using a quarter wave plate.

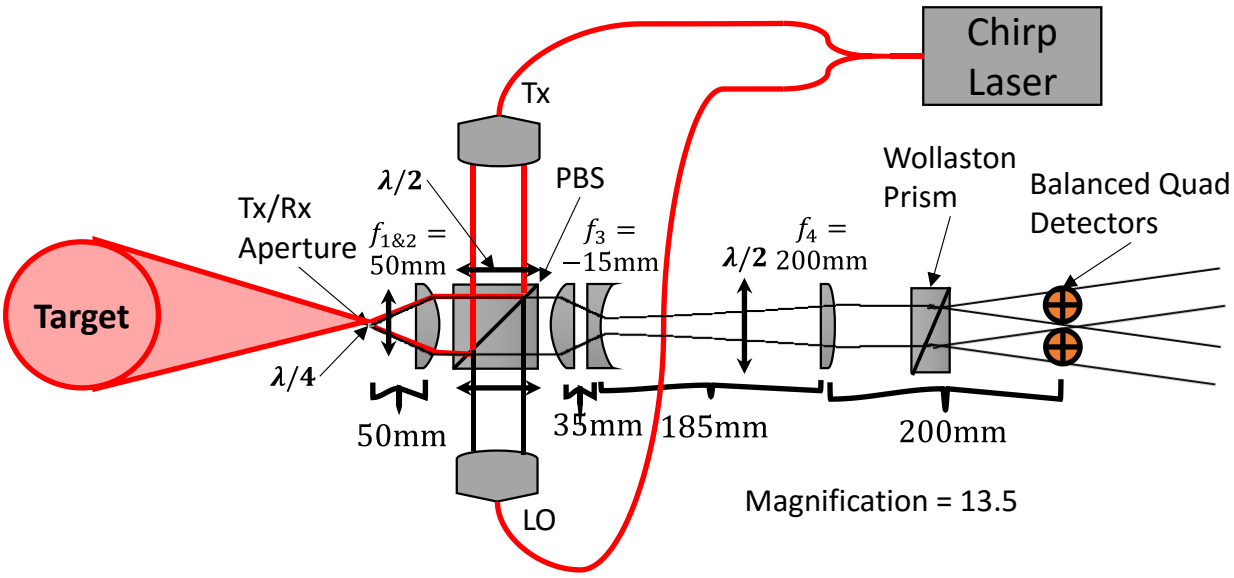

Figure 12 Schematic showing the optical elements for the transmit/receive portion of the DSAL setup.

To the right of the polarizing beam splitter the LO and return light from the target are spatially overlapped but orthogonal in polarization. To coherently mix the LO and return light, a half-wave plate and Wollaston polarizing prism mixes the two polarizations along a 45° axis. This produces two optical paths with equal power of the LO and return signal, but with a 180° phase shift between the LO and the signal light. These two outputs are aligned onto the two quad-cells of a homemade quad-cell autobalanced photoreceiver.

For the DSAL measurement, the aperture is located at the focus of the transmit/receive path to the left of the PBS (see Figure 12). This focus (and the focus of the LO) needed to be imaged onto the quad-cell detector to get separate measurements of the left and right halves of the aperture. The focus size is ~ 35 µm Gaussian radius, to better match the 1 mm diameter of the quad-cell, we

magnified and reimaged the focus onto the quad cell photodiodes. The original design for the Tx\Rx optics used a single 750 mm lens to perform the magnification of the aperture image onto the photodiodes. This caused the back of the system to be 1.5 m in length, which made it very sensitive to vibrations and difficult to pack onto a small breadboard that could be mounted to the stage. A design for a shorter system with sufficient needed magnification was produced.
In the final design, this is accomplished using a series of three lenses on the detector side of optical system. The first lens matches the 50 mm used in the signal and LO paths and is followed by a -15mm and a 200mm lens that reimage the aperture with approximately 13 times magnification. The final system was put together on a 6 inch by 1 foot breadboard. Using 30mm cage components the system is extremely compact and ridged. The sensitivity to vibrations have nearly been eliminated and everything works much smoother.
The final piece of the receiver optics is the quad cell auto balanced detector designed and built in house. The design consists of two quad-cell photodiodes that have the active area split into 4 segments. Each of these segments are independent detectors that are combined using a transistor/op-amp arrangement that feeds back current to keep each paired segment balanced. The outputs of each detector are captured with an 80 Ms/s 8 channel digitizer (Picotechnology).

Task 3.3 Collect Phase History Data w/DSAL

The DSAL collection process is similar to the basic SAL process, except that the signals from multiple detectors are captured simultaneously. For initial testing the targets were placed at a range of 1.83 m at an incline of about 30° to provide range diversity. The computer controlled stage provided a step motion and at each position the heterodyne signal on each quad channel was digitized and Fast Fourier Transformed (FFT) to recover the complex range profile.

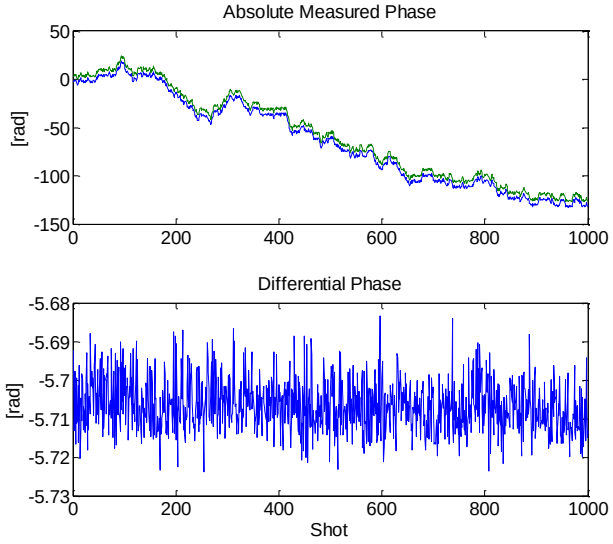

Figure 13 Absolute and differential phase measured to a single retro-reflecting as measured by the DSAL setup.

One of the initial measurements that we took with the DSAL setup was to place a single retro-reflector target in the scene as a phase reference, hold the aperture steady (no motion), and just record the range profile measured by the detectors on either side of the quad-cell. The purpose of this is test whether the differential phase is stable. Figure 13 shows that while over time (about a minute of data collection) the absolute phase on both detector channels drift significantly the measured differential phase is very constant, with RMS fluctuation of about 1/100th of a radian.

Figure 14 shows results for DSAL tests using simple retro-reflecting targets. Some immediate observations of the DSAL imaging technique relative to the SAL+PGA technique was observed with these simple tests, including that the image quality was relatively similar for these simple images; however, unlike with PGA the image cross-range position was quite stable. However, the alignment of the Tx\Rx system for DSAL was critical as sometimes the DSAL image failed where as long as we had measurable signal the SAL image did not.

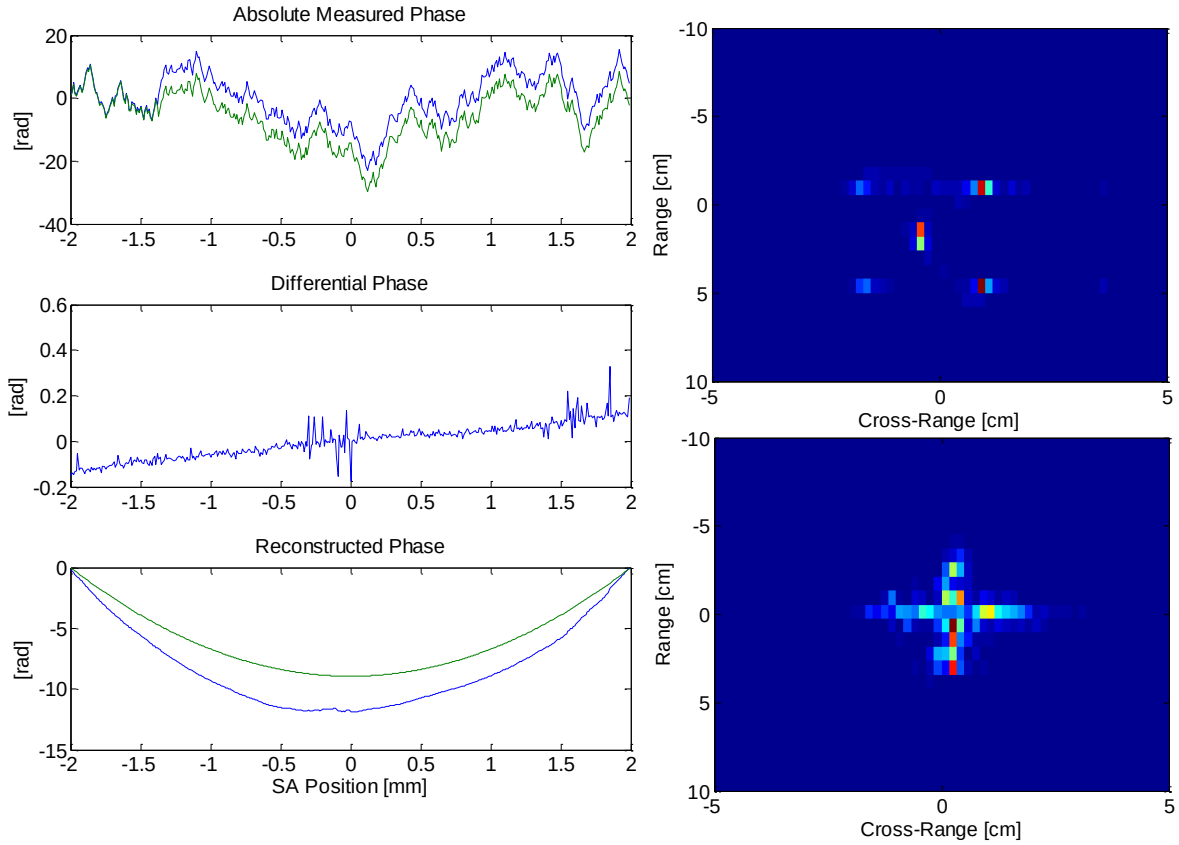

Figure 14 (Left) (top) The measured and unwrapped absolute phase of the left and right side the quadrant detector of a single, isolated, bright retro-reflector target during a synthetic aperture formation. The absolute phase is almost random, but the two phases are well correlated except for a single unwrap difference and the differential phase (middle) shows a nice linear slope corresponding to the cross-range position of the retro-reflector. (Bottom) When integrated, the differential phase produces a quadratic as expected for a straight line aperture motion; however, the quadratic is different than expected for the synthetic aperture motion due to the scaling factor discussed above. (Right, Top) Shows a DSAL image of five retro-reflectors arranged in a X. (Right, Bottom) A DSAL image of a plus sign constructed of retro-tape on a dark background.

Task 3.4 Advanced DSAL techniques.

DSAL Performance Analysis

The original DSAL paper by Stappaerts & Scharlemann in 2005 makes a strong claim about DSAL in the presence of turbulence, "DSAL, unlike SAL, is not affected by turbulence changes near the target." This claim was a strong motivation for our investigation of the DSAL technique, and as will be shown below, it does appear that the DSAL method performs better in the presence of atmospheric turbulence near the target than the standard SAL technique. However, investigating the base DSAL processing method and assumptions the DSAL technique does not provide complete insensitivity to atmospheric turbulence. Writing the 1D DSAL Equation (1) from

Stappaerts & Scharlemann in a compact fashion and including an additional term for atmospheric turbulence near the target we have:

$$E_{\pm,j} = \sum_p a_p \exp i\phi_p(j) \exp\left[\frac{-\left(x_j - x_p\right)^2}{w_o}\right] \exp\left[\frac{-ik\left(x_j - x_p\right)^2}{2R}\right] \exp\left[\frac{-k\left(x_j \pm \frac{d}{4} - x_p\right)^2}{2z}\right],$$

where the $\pm$ refers to the right or left subaperture respectively, j refers to the j^{th} aperture position, a_p is the amplitude of the p^{th} point scatterer, and $\phi_p(j)$ refers to the phase induced by the turbulence on the p^{th} scatterer at the j^{th} aperture position. The standard DSAL processing method is for each aperture position to calculate the differential phase $\Delta\varphi_j = \varphi_{+_j} - \varphi_{-_j}$. There are several equivalent methods to calculate phase differences of complex numbers, the simplest is to find the angle of the conjugate product, i.e. $\Delta\varphi_j = \angle\left\{E_{+_j}E_{-_j}^{*}\right\}$. Looking at the equation above, we see that this results in a product of sums, and while the turbulence phase term falls out in the self-terms (i.e. terms involving the same point scatterer) it does not fall out for terms involving different scatterers. So if the scene contains more than one strong scatterer per resolvable range line, than the turbulent phase evolutions of the different scatterers will convolve together causing errors in the differential phase estimate leading to blurring. To study this further a simple 1D DSAL simulation model was constructed using the 1D DSAL equation above and using a Monte Carlo Kolmogorov phase screen to generate realistic turbulence phase terms $\phi_p(j)$. In this simulation, six point scatterers of two different amplitudes and various spacings were chosen as a scene. Then a 2D phase screen was generated that is the same size of the scene and the phase evolution of each point scatterer was chosen as the column corresponding to the position of the scatterer, x_p, using the hypothesis of Taylor's frozen flow. Running the simulation once and displaying the results for both SAL and DSAL processing we see in Figure 15 that both demonstrate point broadening (if different forms) if the turbulence is sufficiently strong. To better quantify the relative performance we ran the simulation using 100 phase screens and incoherently averaged the result to generate a long duration Point Spread Function (PSF). From this PSF we can calculate numbers roughly equivalent to the Strehl ratio and to the Modulation Transfer Function (MTF) for specific spatial periods. We then ran this simulation for a spread of turbulence strength values (parameterized in terms of Fried's parameter, r_0). The results are presented in Figure 16 and show very little difference in the performance of the DSAL vs. the SAL imaging approach in this situation of moving turbulence near the target. However, this is a 1D simulation with no additional motion errors due to relative transmitter-target motion. What this means is that the DSAL may have advantages in the full 2D situation relative to SAL+PGA, due to providing an independent measurement of the common mode piston phase errors for each range line rather than developing a single collective phase error estimate.

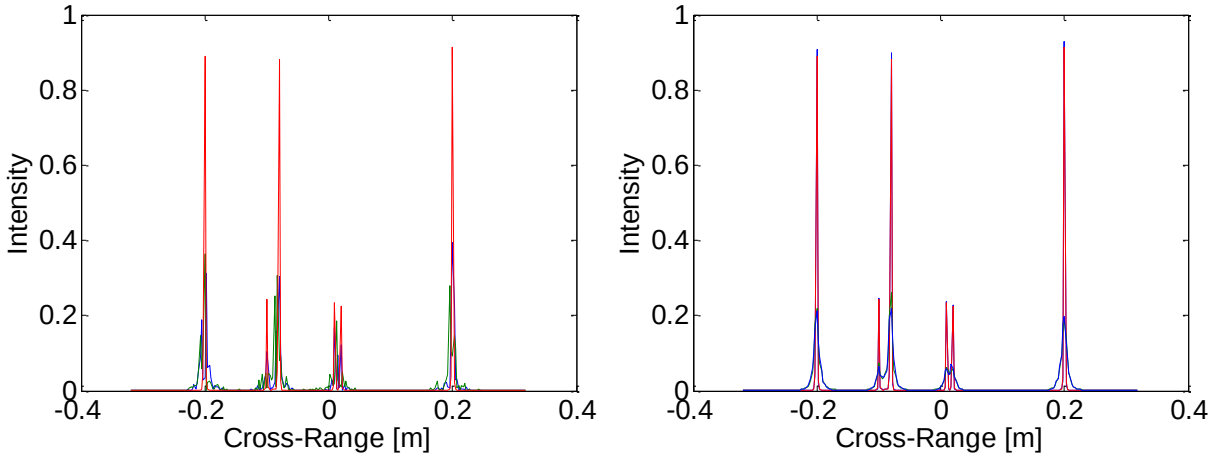

Figure 15 (Left) Single instance of the simulated scene with turbulence value r_0=0.2 m. The green is the DSAL, blue is SAL+PGA, and the red is the SAL with no turbulence. (Right) Simulation of 100 averages. It can be scene that the two small peaks adjacent to one another are just barely resolvable.

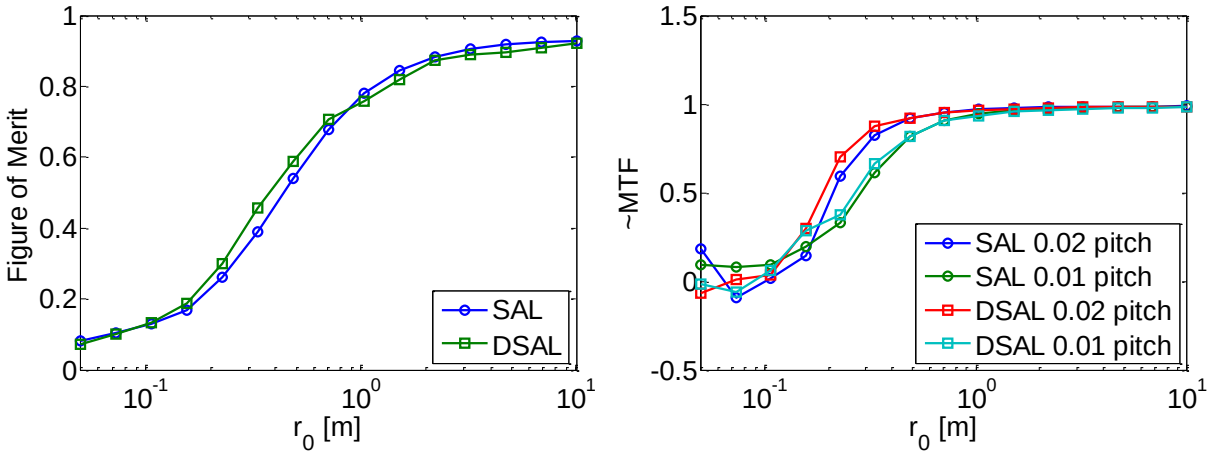

Figure 16 (Left) This shows the average ratio of the peak height of the long term averaged SAL and DSAL signals relative to the value with no turbulence. This is roughly equivalent to the Strehl ratio. (Right) This is the result of the simulation showing the resulting MTF measurement based on the resolvability of the point functions for two different separations.

Task 4: Demonstrate ultra-high resolution SAL imagery.

This task was accomplished by forming high resolution SAL images in an indoor environment with artificially induced optical turbulence. This was not a table-top experiment, that is the FMCW ladar and Tx/Rx receiver was portable, mounted on a standalone cart and the target was mounted to a separate tri-pod. Being indoors the path length was constrained, but a respectable up to 8 m target range was accomplished. The important result of the demonstrations was to compare the performance of DSAL processing with standard SAL+PGA processing with and without turbulence, and with turbulence placed at different locations along the path.

Having figured out that the space heater could be used effectively to mimic turbulence and having an idea of where in the path the turbulence affects the image the most we brought back the retro tape targets to create SAL images. We wanted to see if the DSAL approach would help minimize the effects of turbulence versus the PGA algorithm. Further details of the processing is contained in the CLRC conference paper. Figure 17 shows a series of images all processed using the DSAL or the PGA algorithm. The first images, top left, has no induced turbulence to give a baseline of the image quality. The next image, top right, is with the turbulence near the aperture. There is

slight dimming, blurring, and contrast loss but both the DSAL and PGA processing still produced images very similar to the no turbulence image. The third and fourth images, bottom, has the turbulence in the middle of the path and near the target, respectively. Here we see a strong degradation of both the DSAL and PGA images. However, the DSAL images maintain some recognizable features besides the strong upper triangle feature. The DSAL system can better compensate for phase errors near the target because it removes common mode phase errors for each range line independently whereas the PGA algorithm needs to average over the range lines to estimate the common mode phase error, so when the phase errors vary with range it leads to a corrupted estimate. As discussed above, if there is only one scatterer per range the DSAL compensates for turbulence near the target perfectly, however if there are multiple point scatterers per range their phase errors will mix causing sensitivity to turbulence which has an r_0 smaller than the size of the target.

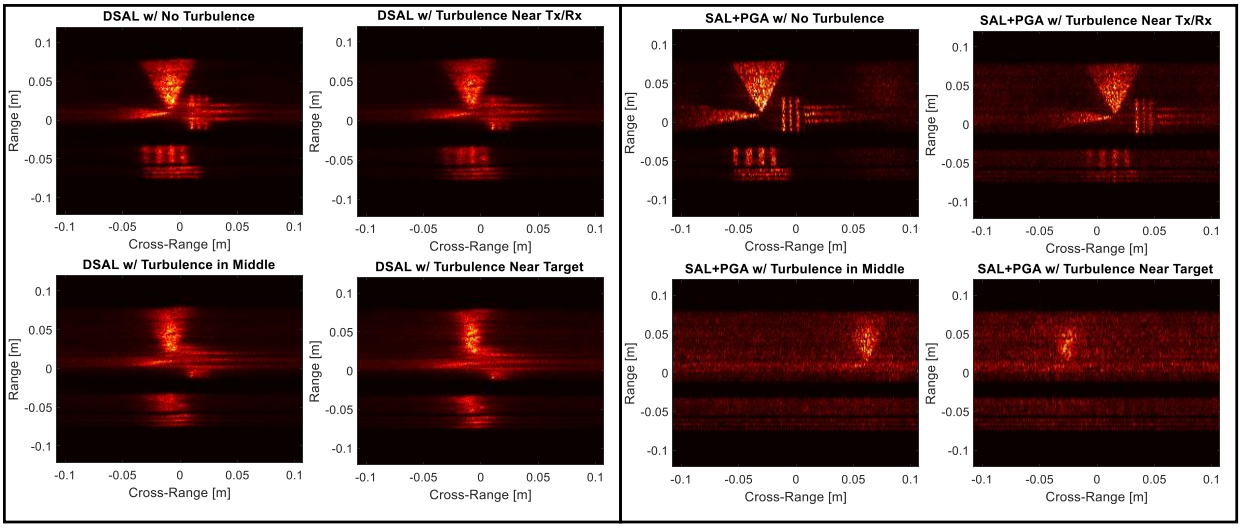

Figure 17 Comparison of DSAL and PGA+SAL processed images for different locations of the induced turbulence on the path.

These demonstrations while indoors, are done in the presence of realistic (if artificially induced) dynamic turbulence, so it is a good test of the potential performance in natural atmospheric turbulence conditions. In fact from our estimates on the C_n^2 values induced by the heater, the turbulence is quite strong and similar to what would be observed during daytime for relatively long horizontal paths. In fact the r_0 of < 5 cm measured above is smaller than the standard 5 – 10 cm expected for vertical path viewing at sea level. Due to the weak sensitivity to turbulence near the Tx/Rx, SAL+PGA and DSAL seem well suited to ground based applications for vertical or upward slant path imaging.

References

[1] M. Bashkansky, "Synthetic aperture imaging at 1.5μ: laboratory demonstration and potential application to planet surface studies," 2002, vol. 4849, pp. 48–56.

[2] S. M. Beck, J. R. Buck, W. F. Buell, R. P. Dickinson, D. A. Kozlowski, N. J. Marechal, and T. J. Wright, "Synthetic-aperture imaging laser radar: laboratory demonstration and signal processing," *Appl. Opt.*, vol. 44, no. 35, pp. 7621–7629, Dec. 2005.

[3] B. W. Krause, J. Buck, C. Ryan, D. Hwang, P. Kondratko, A. Malm, A. Gleason, and S. Ashby, "Synthetic aperture ladar flight demonstration," in *2011 Conference on Lasers and Electro-Optics (CLEO)*, 2011, pp. 1–2.

[4] P. A. Roos, R. R. Reibel, T. Berg, B. Kaylor, Z. W. Barber, and W. R. Babbitt, "Ultrabroadband optical chirp linearization for precision metrology applications," *Optics Letters*, vol. 34, no. 23, p. 3692, Nov. 2009.

[5] Z. W. Barber and S. Crouch, "Table-Top Explorations of Synthetic Aperture Ladar Imaging," 2013, p. CTu1H.2.

[6] L. C. Andrews and R. L. Phillips, *Laser beam propagation through random media*, 2nd ed. Bellingham, Wash: SPIE Press, 2005.

[7] S. Crouch and Z. W. Barber, "Laboratory demonstrations of interferometric and spotlight synthetic aperture ladar techniques," *Opt. Express*, vol. 20, no. 22, pp. 24237–24246, Oct. 2012.

[8] E. A. Stappaerts and E. T. Scharlemann, "Differential synthetic aperture ladar," *Opt. Lett.*, vol. 30, no. 18, pp. 2385–2387, Sep. 2005.

[9] E. A. Stappaerts, "Differential optical synthetic aperture radar," US6879279 B2, 12-Apr-2005.

[10] Z. W. Barber and J. R. Dahl, "Synthetic aperture ladar imaging demonstrations and information at very low return levels," *Applied Optics*, vol. 53, no. 24, p. 5531, Aug. 2014.

1.

1. Report Type

Final Report

Primary Contact E-mail

Contact email if there is a problem with the report.

barber@spectrum.montana.edu

Primary Contact Phone Number

Contact phone number if there is a problem with the report

4069945925

Organization / Institution name

Montana State University

Grant/Contract Title

The full title of the funded effort.

(YIP) Synthetic Aperture Ladar Imaging and Atmospheric Turbulence

Grant/Contract Number

AFOSR assigned control number. It must begin with "FA9550" or "F49620" or "FA2386".

FA9550-12-1-0421

Principal Investigator Name

The full name of the principal investigator on the grant or contract.

Zeb William Barber

Program Manager

The AFOSR Program Manager currently assigned to the award

Julie Moses

Reporting Period Start Date

08/01/2012

Reporting Period End Date

05/31/2016

Abstract

This is the final technical report for the Air Force Office of Scientific Research Young Investigator Program (YIP) project entitled "Synthetic Aperture Ladar and Atmospheric Turbulence". It includes a technical summary of the entire effort and a more detailed description of the final portion of the effort. The overall objectives of the effort were to utilize high resolution FMCW ladar techniques for high resolution synthetic aperture ladar (SAL) imaging as a tool for investigating atmospheric turbulence, and investigating the effect of atmospheric turbulence on coherent ladar and SAL imaging. The main concept for investigating turbulence using the high resolution FMCW ladar was to use range resolved point targets (retroreflectors) as beacons in a two-way ladar measurement system. The statistics of the phase and amplitude fluctuations of the beacon signals can then be used to measure the strength of the optical turbulence in the path. In addition, to investigating the effects of atmospheric turbulence on SAL imaging through simulation, optical hardware was constructed to implement and investigate the Differential Synthetic Aperture Ladar (DSAL) imaging, which may have advantages over standard SAL imaging in the presence of turbulence near the target. In the period since the last progress report, we have improved the DSAL hardware and performed comparison measurements between more standard SAL imaging and DSAL in the presence of different atmospheric turbulence conditions. Also during this final period we improved upon the measurement setup and data processing methods for the FMCW ladar based atmospheric turbulence measurement tool that

allows us to have better confidence in our measurement of atmospheric turbulence.

Distribution Statement

This is block 12 on the SF298 form.

Distribution A - Approved for Public Release

Explanation for Distribution Statement

If this is not approved for public release, please provide a short explanation. E.g., contains proprietary information.

SF298 Form

Please attach your SF298 form. A blank SF298 can be found here. Please do not password protect or secure the PDF The maximum file size for an SF298 is 50MB.

AF SF298.pdf

Upload the Report Document. File must be a PDF. Please do not password protect or secure the PDF . The maximum file size for the Report Document is 50MB.

AFYIP Final Report_Final.pdf

Upload a Report Document, if any. The maximum file size for the Report Document is 50MB.

Archival Publications (published) during reporting period:

Barber, Z. W. and Dahl, J. R. "Experimental Demonstration of Differential Synthetic Aperture Ladar" CLEO: Science and Innovations 2015 (2015): STh3O.3. doi:10.1364/CLEO_SI.2015.STh3O.3, Available at https://www.osapublishing.org/abstract.cfm?uri=CLEO_SI-2015-STh3O.3

Crouch, S., Kaylor, B. M., Barber, Z. W., and Reibel, R. R. "Three Dimensional Digital Holographic Aperture Synthesis" Optics Express 23, no. 18 (2015): 23811. doi:10.1364/OE.23.023811, Available at https://www.osapublishing.org/abstract.cfm?URI=oe-23-18-23811 (Z.W. Barber's contributions).

2. New discoveries, inventions, or patent disclosures:
Do you have any discoveries, inventions, or patent disclosures to report for this period?

No

Please describe and include any notable dates

Do you plan to pursue a claim for personal or organizational intellectual property?

Changes in research objectives (if any):

None

Change in AFOSR Program Manager, if any:

Program Manager was changed from Kent Miller to Julie Moses in July 2013.

Extensions granted or milestones slipped, if any:

A no cost extension of 9 months was granted with consideration for the Air Force extend effort in coherent ladar based atmospheric turbulence characterization and imaging and transition developments to an AF SBIR and subcontract to work with EO sensors group at Wright-Patterson AFB.

AFOSR LRIR Number

LRIR Title

Reporting Period

Laboratory Task Manager

Program Officer

Research Objectives

Technical Summary

Funding Summary by Cost Category (by FY, $K)

	Starting FY	FY+1	FY+2
Salary			
Equipment/Facilities			
Supplies			
Total			

Report Document

Report Document - Text Analysis

Report Document - Text Analysis

Appendix Documents

2. Thank You

E-mail user

Jun 03, 2016 18:08:26 Success: Email Sent to: barber@spectrum.montana.edu